Theory of optical spin orientation in silicon

J. L. Cheng,[1,2] J. Rioux,[1] J. Fabian,[3] and J. E. Sipe[1,*]

[1]*Department of Physics and Institute for Optical Sciences, University of Toronto, 60 St. George Street, Toronto, Ontario, Canada M5S 1A7*
[2]*Hefei National Laboratory for Physical Sciences at Microscale, University of Science and Technology of China, Hefei, Anhui, 230026, China*
[3]*Institute for Theoretical Physics, University of Regensburg, 93040 Regensburg, Germany*

Despite weak spin-orbit coupling and an indirect band gap, significant optical spin orientation is possible in silicon. We show this by performing full band-structure calculations of the phonon-assisted absorption of circularly polarized light in bulk silicon. At 4 K a maximum spin polarization of 25% is found at the band edge; at room temperature the polarization is still 15%. We present the selection rules and give the contributions from the individual phonon branches, valence bands, and conduction band valleys. Dominant are the TO/LO phonon-assisted transitions from the heavy-hole to the conduction band.

PACS numbers: 72.25.Fe,78.20.-e

arXiv:1011.2259v1 [cond-mat.mtrl-sci] 10 Nov 2010

Introduction. Silicon is an interesting material for spintronics due to its mature technology and long electron spin relaxation time [1], which exceeds a microsecond below 50 K and is about 10 ns at room temperature [1–3]. A prerequisite for silicon-based spin devices is the effective injection of spins. Of the two important methods of generating spin accumulation, optical and electrical, the latter has already been demonstrated in silicon [4–7] and studied theoretically [8, 9]. Much earlier, the first spin injection experiment involved optical absorption across the indirect gap in silicon [10]. Yet optical spin injection, called optical (spin) orientation [11], has generally been restricted to the study of spin properties of direct gap semiconductors such as GaAs. In silicon, because the indirect transition requires phonon mediation and the spin-orbit coupling is weak, optical orientation is thought of as ineffective, despite the lack of realistic calculations. Here we give the selection rules at the indirect gap for optical orientation in silicon, and determine the degree of spin polarization for a range of photon energies above the indirect gap. We find that spin can be generated optically with a significant (more than 10%) spin polarization, even at room temperature. Such a robust optical spin orientation could be probed either electrically or optically.

We study the degree of spin polarization (DSP) of the conduction electrons in silicon under an incident circularly polarized light with photon energy below the direct gap, and derive the selection rules for each phonon-assisted process without the restrictive assumptions adopted by Li and Dery [12] in their recent study of optical luminescence, the reverse process of optical orientation. We find that the DSP depends strongly on the phonon branch that mediates the optical transition. Using an empirial pseudopotential model (EPM) [13, 14] for the electronic states, and an adiabatic bond charge model (ABCM) [15] for phonons, the calculated maximum DSP is about -25% at the injection edge at 4 K and -15% at 300 K, exhibiting strong valley anisotropy.

General features. For an incident laser beam with field $\mathbf{E}(t) = \mathbf{E}_\omega e^{-i\omega t} + c.c.$ in the medium, the time rate of change of the expectation value of any observable $\hat{A}$ due to indirect absorption can be written as $\dot{A} = \mathcal{A}^{ab} E^a_\omega E^{b*}_\omega$, where $\mathcal{A}^{ab} = \sum_I \mathcal{A}^{ab}_I$ and $\mathcal{A}^{ab}_I = \sum_{cv\lambda\pm} \mathcal{A}^{ab}_{I;cv\lambda\pm}$ is the coefficient for injection into the Ith valley ($I = X, \bar{X}, Y, \bar{Y}, Z, \bar{Z}$ in bulk silicon); $\mathcal{A}^{ab}_{I;cv\lambda\pm}$ gives the contribution from conduction band c, valence band v, phonon branch λ (longitudinal optical (LO) and acoustic (LA), and transverse optical (TO) and acoustic (TA) branches), and phonon process (+ for emission, − for absorption). From Fermi's golden rule we have

$$\begin{aligned}\mathcal{A}^{ab}_{I;cv\lambda\pm} &= \frac{2\pi}{\hbar}\sum_{\mathbf{k}_c\epsilon I,\mathbf{k}_v}\delta(\varepsilon_{c\mathbf{k}_c} - \varepsilon_{v\mathbf{k}_v} \pm \hbar\Omega_{(\mathbf{k}_c-\mathbf{k}_v)\lambda} - \hbar\omega)\\ &\quad\times N_{(\mathbf{k}_c-\mathbf{k}_v)\lambda\pm}\mathcal{A}^{ab}_{c\mathbf{k}_c v\mathbf{k}_v\lambda}, \qquad (1)\\ \mathcal{A}^{ab}_{c\mathbf{k}_c v\mathbf{k}_v\lambda} &= \sum_{\sigma_c\sigma'_c\sigma_v} A_{\bar{c}'\bar{c}\mathbf{k}_c} T^a_{\bar{c}\mathbf{k}_c\bar{v}\mathbf{k}_v\lambda}\left(T^b_{\bar{c}'\mathbf{k}_c\bar{v}\mathbf{k}_v\lambda}\right)^*.\end{aligned}$$

Here $\bar{v} = (v, \sigma_v)$ denotes a valence band state with band index v and spin index σ_v; $\bar{c} = (c, \sigma_c)$ and $\bar{c}' = (c, \sigma'_c)$ denote conduction band states with the same band index c. By $\mathbf{k}_c\epsilon I$ we mean the summation is only over the Ith valley, $\varepsilon_{n\mathbf{k}}$ ($n = c, v$) is the energy of the electron state $|n\mathbf{k}\rangle$, $\hbar\Omega_{\mathbf{q}\lambda}$ gives the phonon energy at wave vector $\mathbf{q}$ and mode λ, and $N_{\mathbf{q}\lambda\pm} = N_{\mathbf{q}\lambda} + \frac{1}{2} \pm \frac{1}{2}$, where $N_{\mathbf{q}\lambda}$ is the indicated equilibrium phonon number. Here we only consider the spin properties of the injected electrons, and $A_{\bar{c}'\bar{c}\mathbf{k}_c} = \langle\bar{c}'\mathbf{k}_c|\hat{A}|\bar{c}\mathbf{k}_c\rangle$ gives the matrix element of $\hat{A}$ between conduction band states; $T^a_{\bar{c}\mathbf{k}_c\bar{v}\mathbf{k}_v\lambda} = \frac{e}{\omega}\langle\bar{c}\mathbf{k}_c|H^{ep}_{(\mathbf{k}_c-\mathbf{k}_v)\lambda}(\hbar\omega - H^e + \varepsilon_{v\mathbf{k}_v})^{-1}v^a + v^a(\varepsilon_{c\mathbf{k}_c} - H^e - \hbar\omega)^{-1}H^{ep}_{(\mathbf{k}_c-\mathbf{k}_v)\lambda}|\bar{v}\mathbf{k}_c\rangle$ is the ath component of the indirect transition matrix element; $H^{ep}_{\mathbf{q}\lambda}$ is given from the electron-phonon interaction Hamiltonian $H^{ep} = \sum_{\mathbf{q},\lambda}(a_{\mathbf{q}\lambda} + a^\dagger_{-\mathbf{q}\lambda})H^{ep}_{\mathbf{q}\lambda}$, where $a_{\mathbf{q}\lambda}$ is the phonon annihilation operator; H^e is the unperturbed single-particle electron Hamiltonian, and $v^a = \partial H^e/\partial p^a$

is the electron velocity operator. Equation (1) is similar to the luminescence intensity expression used by Li and Dery [12], except for the reversed initial and final states.

By taking $\hat{A}$ as the operator for the electron number density or the density of the fth spin component, from $\mathcal{A}^{ab}$ we get the optical injection rate coefficients respectively of electrons, ξ^{ab}, and the fth spin component, ζ^{fab}, respectively a second rank tensor and a third rank pseudotensor. For bulk silicon, the electron states in each conduction valley have only C_{4v} symmetry; for excited electrons in the Z valley there are only two independent nonzero components of each response coefficient, $\xi_Z^{xx} = \xi_Z^{yy} \equiv \xi^{(1)}$ and $\xi_Z^{zz} \equiv \xi^{(2)}$ for ξ_Z^{ab}, and $\zeta_Z^{zxy} = -\zeta_Z^{zyx} \equiv i\zeta^{(1)}$ and $\zeta_Z^{xyz} = -\zeta_Z^{yxz} = (\zeta_Z^{xzy})^* = -(\zeta_Z^{yzx})^* \equiv i\zeta^{(2)}$ for ζ_Z^{fab}. The injection coefficients for electrons in the other valleys can be obtained by properly rotating the Z valley to the other valleys. The total injection coefficients satisfy

$$\begin{aligned} \xi^{xx} &= \xi^{yy} = \xi^{zz} \equiv \xi, \\ \zeta^{xyz} &= \zeta^{yzx} = \zeta^{zxy} = -\zeta^{xzy} = -\zeta^{zyx} = -\zeta^{yxz} \equiv i\zeta, \end{aligned} \tag{2}$$

with $\xi = 2\xi^{(2)} + 4\xi^{(1)}$ and $\zeta = 2\zeta^{(1)} + 4\text{Re}\zeta^{(2)}$. All the $\xi^{(i)}$ and $\zeta^{(i)}$ are real except $\zeta^{(2)}$.

Selection rules. We now look at the selection rules for $\mathbf{T}_{\bar{c}\mathbf{k}_c^0\bar{v}\mathbf{k}_v^0\lambda}$ at the absorption edge where $\mathbf{k}_v^0 = 0$ and $\mathbf{k}_c^0 \approx 0.85\overrightarrow{\Gamma X}$. While Li and Dery [12] examined these assuming that only certain intermediate states made significant contributions to $\mathbf{T}_{\bar{c}\mathbf{k}_c^0\bar{v}\mathbf{k}_v^0\lambda}$, we identify the selection rules more generally based only on the symmetry of the crystal. We begin with the electron states that lie in the Z valley. For the C_{4v} symmetry group identified by the $\mathbf{q}^Z \equiv \mathbf{k}_c^0 - \mathbf{k}_v^0$ axis, $H_{\mathbf{q}^Z\lambda}^{ep}$ has the symmetry Δ_1 for LA branch, (with basis functions z), Δ_2' for LO branch, $(x^2 - y^2)$, and Δ_5 for both TA and TO branches ($\{x, y\}$).

$\boldsymbol{T}_{c\boldsymbol{k}_c^0 v\boldsymbol{k}_v^0}^{\lambda}$	TA/TO		LA	LO
	x	y	z	$x^2 - y^2$
$\lvert\mathcal{X}\rangle$	0	$(0, 0, T_1^{(\prime)})$	$(0, T_3, 0)$	$(T_4, 0, 0)$
$\lvert\mathcal{Y}\rangle$	$(0, 0, T_1^{(\prime)})$	0	$(T_3, 0, 0)$	$(0, T_4, 0)$
$\lvert\mathcal{Z}\rangle$	$(0, T_2^{(\prime)}, 0)$	$(T_2^{(\prime)}, 0, 0)$	0	$(0, 0, T_5)$

TABLE I: Selection rules of $\boldsymbol{T}_{c\boldsymbol{k}_c^0 v\boldsymbol{k}_v^0\lambda}$. Unprimed (primed) quantities are for TA (TO) phonon.

Without including spin, the valence states at Γ have Γ_{25}' symmetry (basis functions $\{yz, zx, xy\}$, which we label here as $\{\mathcal{X}, \mathcal{Y}, \mathcal{Z}\}$), while the conduction band edge state as Δ_1 symmetry (basis function $\{z\}$) [16]. By applying all the symmetry operations we can identify the nonzero components in $\mathbf{T}_{\bar{c}\mathbf{k}_c^0\bar{v}\mathbf{k}_v^0\lambda}$, given in Table I. While for direct gap injection in a cubic crystal there is only one nonzero matrix element, here seven nonzero elements are allowed because of the reduced symmetry of the conduction band at $\mathbf{k}_c^0$ and the involvement of phonons. In Li and Dery's more restricted analysis [12], T_5, T_2, and T_2' vanish.

τ		TA/TO	LA	LO
SO	$\bar{\zeta}$	$(0, -\frac{2}{3}{T_1^{(\prime)}}^* T_2^{(\prime)})$	$(-\frac{2}{3}\lvert T_3\rvert^2, 0)$	$(\frac{2}{3}\lvert T_4\rvert^2, \frac{2}{3}T_4T_5^*)$
	$\bar{\xi}$	$(\frac{2}{3}\lvert T_2^{(\prime)}\rvert^2, \frac{4}{3}\lvert T_1^{(\prime)}\rvert^2)$	$(\frac{2}{3}\lvert T_3\rvert^2, 0)$	$(\frac{2}{3}\lvert T_4\rvert^2, \frac{2}{3}\lvert T_5\rvert^2)$
LH,HH	$\bar{\zeta}$	$(0, \frac{1}{3}{T_1^{(\prime)}}^* T_2^{(\prime)})$	$(\frac{1}{3}\lvert T_3\rvert^2, 0)$	$(-\frac{1}{3}\lvert T_4\rvert^2, -\frac{1}{3}T_4T_5^*)$
	$\bar{\xi}$	$(\frac{2}{3}\lvert T_2'\rvert^2, \frac{4}{3}\lvert T_1'\rvert^2)$	$(\frac{2}{3}\lvert T_3\rvert^2, 0)$	$(\frac{2}{3}\lvert T_4\rvert^2, \frac{2}{3}\lvert T_5\rvert^2)$

TABLE II: Band edge transition rates $(\bar{\mathcal{A}}_{cv\tau}^{(1)}, \bar{\mathcal{A}}_{cv\tau}^{(2)})$ with $\mathcal{A}$ being ξ for carrier injection and ζ for spin injection.

Including spin, the valence states at Γ are split by spin-orbit coupling into heavy hole (HH), light hole (LH), and split-off (SO) states, respectively $\left|\frac{3}{2}, \pm\frac{3}{2}\right\rangle = \mp\lvert\mathcal{X} \pm i\mathcal{Y}\rangle\lvert\pm\rangle/\sqrt{2}$, $\left|\frac{3}{2}, \pm\frac{1}{2}\right\rangle = \sqrt{2/3}\lvert\mathcal{Z}\rangle\lvert\pm\rangle \mp \lvert\mathcal{X} \pm i\mathcal{Y}\rangle\lvert\mp\rangle/\sqrt{6}$, and $\left|\frac{1}{2}, \pm\frac{1}{2}\right\rangle = \pm\lvert\mathcal{Z}\rangle\lvert\pm\rangle/\sqrt{3} + \lvert\mathcal{X} \pm i\mathcal{Y}\rangle\lvert\mp\rangle/\sqrt{3}$ in standard notation, with the SO states split off $\Delta_{so} = 44$ meV from the degenerate HH and LH states [17]. At the conduction band edge, the states can be approximately written as $\lvert z\pm\rangle$ due to the very small spin mixing. At band edge, the injection rates can be identified by $\bar{\mathcal{A}}_{Z;cv\tau}^{ab} = \sum_{\lambda\in\tau}\mathcal{A}_{Z;c\boldsymbol{k}_c^0 v\boldsymbol{k}_v^0\lambda}^{ab}$; here τ indicates the phonon type (TA, TO, LA, LO), $\sum_{\lambda\in\tau}$ indicates the summation over all modes in τ^{th} branch. The $\bar{\mathcal{A}}_{Z;cv\tau}^{ab}$ have the same symmetry as the $\mathcal{A}_Z^{ab}$, and their nonzero components are correspondingly labeled as $\bar{\mathcal{A}}_{cv\tau}^{(1,2)}$ and listed in Table II.

The selection rules summarized in Table II for carrier and spin injection obey some properties that are reminiscent of the selection rules for injection across the direct gap: (i) the carrier injection terms $\bar{\xi}_{cv\tau}^{(1,2)}$ are the same for each valence band; (ii) the spin injection terms $\bar{\zeta}_{cv\tau}^{(1,2)}$ are the same for $v = HH$ and LH [18]; the valence band sum $\sum_v \bar{\zeta}_{cv\tau}^{(1,2)} = 0$. The last result does *not* imply that the injected spin polarization vanishes when the laser pulse is wide enough to involve all valence bands, because the density of states for each valence band is different. Nonetheless, with increasing excitation energy the relevant hole states typically involve a superposition of many band edge hole states, and the DSP tends to decrease rapidly due to the vanishing of the valence band sum.

Results. However, there are important differences between the spin injection due to direct and indirect absorption. Here we analyze a particular experimental configuration where σ^- light, $\mathbf{E}_\omega = E_o(\hat{\mathbf{x}} - i\hat{\mathbf{y}})/\sqrt{2}$ is incident on silicon. The six conduction band valleys can be divided into two sets, one consisting of Z and $\bar{Z}$, and the other of $X, \bar{X}, Y$, and $\bar{Y}$. The valleys in each set all have the

same injection rates, which are

$$\dot{n}_Z = \xi^{(1)} |E_o|^2 , \quad \dot{S}^z_Z = -\zeta^{(1)} |E_o|^2 ,$$
$$\dot{n}_X = \frac{\xi^{(1)} + \xi^{(2)}}{2} |E_o|^2 , \quad \dot{S}^z_X = -\mathrm{Re}[\zeta^{(2)}] |E_o|^2 ,$$

with $\dot{S}^{x,y}_I = 0$ for all I. Therefore the injected spin in each valley points either along z or $-z$. The degree of spin polarization (DSP) is defined as $\dot{S}/(\hbar\dot{n}/2)$. At the onset of absorption the selection rules show that different phonon-assisted processes result in different spin polarizations: the TA/TO phonon-assisted process only injects spins in the $X, \bar{X}, Y, \bar{Y}$ valleys, the LA phonon-assisted process injects spins only in the $Z, \bar{Z}$ valleys, and the LO phonon-assisted process injects spins in all valleys but with different magnitudes. There seems to be no way to analyze the indirect transitions by considering them as virtual direct transitions followed by a phonon process that does not affect the spin, a strategy implicit in the work of Lampel [19–21]. Since even at the onset of absorption the states involved are not eigenstates of spin, the insensitivity of the electron-phonon coupling to electron spin does not guarantee that this approach is correct, and indeed the spin injections into the Z and X valleys, for example, are totally different. It seems unproductive to try to define an explicit DSP for each phonon process, since some of these processes are determined by more than one nonzero parameter.

For quantitative calculations of the injection rate near and away from the onset of absorption we use electron [3, 12] and phonon [15] states with parameters set used earlier [3]; the indirect gap is $E_{ig} = 1.17$ meV, and the phonon energies on the onset of absorption are 19 (TA), 47 (LA), 53 (LO), and 57 (TO) meV. Depending on whether phonons are absorbed or emitted, the injection edge is shifted to lower or higher energy. Thus the injection spectrum starts with the TA phonon-assisted process at low temperature, where only phonon emission can occur, and with the TO phonon-assisted process at high temperature, where the absorption process becomes important. Because the TA and TO phonons have the same symmetry properties, the structure of the injection edge is similar at all temperatures. From our calculations, the LA phonon-assisted process with its low injection rate is always ignorable. The carrier injection is dominated by the TO phonon-assisted process, while the spin injection is dominated by TO and LO phonon-assisted processes with generally comparable contributions. Due to the densities of states, injection from the HH band is more important than that from the LH band, and that from the SO band is least important.

We focus on the DSP in this letter. Fig. 1 gives the main results of DSP spectra (solid curves) at temperature 4 K (a) and 300 K (b). At 4 K, the injection edge shifts from the band gap to $\hbar\omega_2 = E_{ig} + \Omega_{\boldsymbol{k}_c^0,\mathrm{TA}}$, due to the energy involved in the TA phonon emission process. The

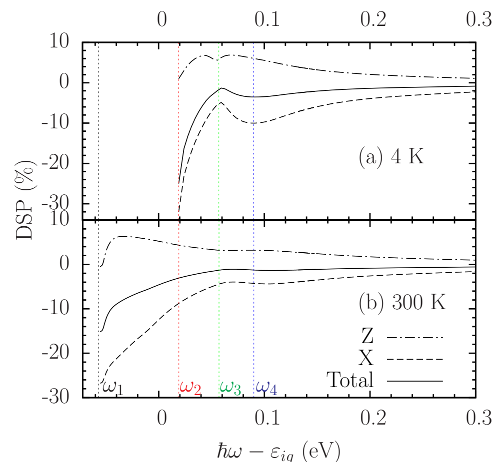

FIG. 1: (color online). DSP spectra at 4 and 300 K for the spins in Z/X valley and the total spin.

spectrum starts at -25% at the injection edge, decreases to a local minimum ≈ 0 at $\hbar\omega_3 \approx E_{ig} + \Omega_{\boldsymbol{k}_c^0\mathrm{TO}}$, then increases to a local maximum -5% at $\hbar\omega_4 \approx E_{ig} + 90$ meV, and then decreases monotonically to zero. In contrast, at 300 K the injection edge is at $\hbar\omega_1 = E_{ig} - \Omega_{\boldsymbol{k}_c^0,\mathrm{TO}}$ because the TO phonon absorption process takes effect at high temperature, and DSP decrease nearly monotonically from the injection edge value -16% to zero at high photon energy; The peak appearing at 4 K becomes obscured. Note that indirect spin injection is more effective than the direct gap spin injection at $\boldsymbol{k}_c^0$, for which DSP is less than 1% [18]. The DSP spectra for Z (dot-dashed curves) and X (dashed curves) valleys are also plotted in the same figure, and they show totally different behavior; they even have opposite polarization directions, consistent with Li and Dery's conclusion [12] that the luminescence from these two valleys have opposite degree of circular polarization. The DSP spectrum for X valley is similar to the total but with larger values; *e.g.*, the injection edge values are -32% at 4 K and -28% at 300 K, while the DSP for Z valley show different photon energy dependence. So it should be possible to obtain a much larger DSP in confined silicon structures in which the valley degeneracy is broken. All DSP are less than 5% for photon energies over $E_{ig} + 0.3$ eV, and decrease rapidly to zero for all temperatures.

To better understand these results, the DSP spectra at 4 K are plotted in Fig. 2 for the transition from each phonon branch and each valence band. The injection edge at $E_{ig} + \Omega_{\boldsymbol{k}_c^0\lambda}$ is clear for each phonon branch. For the X valley, for $\omega \in [\omega_2, \omega_3]$, the TA phonon-assisted process dominates and gives the fast decrease; for $\omega \in [\omega_3, \omega_4]$, the TO phonon-assisted process takes effect and gives much larger spin injection rates, and leads to the peak at ω_4; for $\omega > \omega_4$, all phonon branches contribute, and the DSP decreases. A similar explanation can be found for the DSP for Z valley. At 300 K, the TO/LO

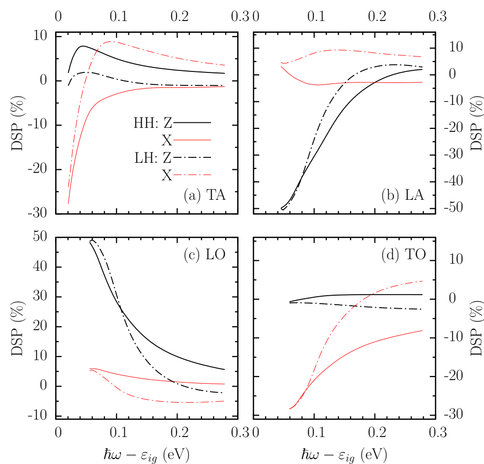

FIG. 2: (color online) DSP spectra from different transition process for Z (black thick curves) and X valley (red thin curves) at 4 K. Solid/dot-dashed curves are the injection from HH/LH valence band. The vertical scale in (b) and (d) are on the right-hand side.

phonon absorption processes dominate the injection edge and obscure the peak.

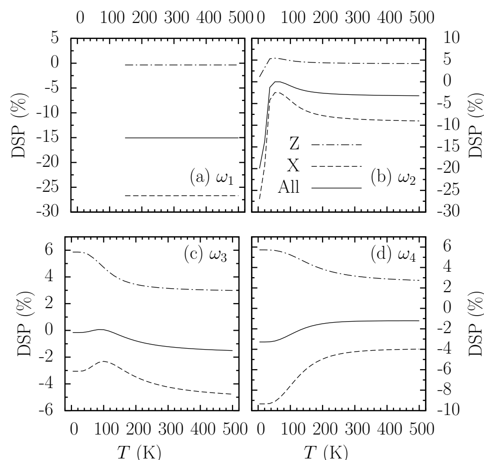

FIG. 3: (color online). Temperature dependence of DSP for Z (dot-dashed curves)/X valley(dashed curves)/total (solid curves) at photon energies ω_{1-4}. The vertical scale in (b) and (d) are on the right-hand side.

Fig. 3 gives the temperature dependence of DSP at the special photon energies ω_{1-4} given in Fig. 1. Around band edge, the temperature dependence of all rates considered here only comes from phonon numbers $N_{\boldsymbol{q}\lambda} \approx N_{\boldsymbol{k}_c^0\lambda}$, so each injection rate increases with temperature. For the injection at photon energy ω_1 [Fig. 3 (a)], only the TO phonon absorption process takes effect; the phonon numbers involved in carrier and spin injection rates are the same and cancel out in the DSP, which results in its temperature independence. Furthermore, this temperature independence holds for the DSP from each phonon assisted transition process. However, because the temperature dependence of $N_{\boldsymbol{q}\lambda}$ is different for each phonon branch, their relative contributions to the spin and carrier injection rates change with temperature, leading to the temperature dependence of the total DSP given in Fig. 3 (b) to (d); $N_{\boldsymbol{q}\lambda} \propto T$ at high temperature, so the injection coefficients $\mathcal{A}$ are approximately proportional to T themselves, and lead to a saturated DSP.

In summary, we have calculated the optically generated spin polarization of the conduction electrons in bulk silicon and presented its temperature dependence, valley anisotropy, and phonon-mode contribution. We believe that our findings of robust optical spin orientation in silicon will now encourage optical experiment on the spin properties in silicon.

This work was supported by the Natural Sciences and Engineering Research Council of Canada. J.L.C acknowledges support from China Postdoctoral Science Foundation. J.R. acknowledges support from FQRNT. J.F. acknowledges support from DFG SPP1285.

* Author to whom correspondence should be addressed; Electronic address: sipe@physics.utoronto.ca

[1] J. Fabian, A. M.-Abiague, C. Ertler, P. Stano, and I. Žutić, Acta Phys. Slovaca **57**, 565 (2007).
[2] B. Huang, D. J. Monsma, and I. Appelbaum, Phys. Rev. Lett. **99**, 177209 (2007).
[3] J. L. Cheng, M. W. Wu, and J. Fabian, Phys. Rev. Lett. **104**, 016601 (2010).
[4] I. Appelbaum, B. Huang, and D. J. Monsma, Nature **447**, 295 (2007).
[5] B. T. Jonker, G. Kioseoglou, A. T. Hanbicki, C. H. Li, and P. E. Thompson, Nature Phys. **3**, 542 (2007).
[6] S. P. Dash, S. Sharma, R. S. Patel, M. P. de Jong, and R. Jansen, Nature **462**, 491 (2009).
[7] L. Grenet, M. Jamet, P. Noe, V. Calvo, J. M. Hartmann, L. E. Nistor, B. Rodmacq, S. Auffret, P. Warin, and Y. Samson, Appl. Phys. Lett. **94**, 032502 (2009).
[8] I. Žutić, J. Fabian, and S. C. Erwin, Phys. Rev. Lett. **97**, 026602 (2006).
[9] P. Mavropoulos, Phys. Rev. B **78**, 054446 (2008).
[10] G. Lampel, Phys. Rev. Lett. **20**, 491 (1968).
[11] Optical Orientation (North-Holland, New York, 1984), eds. F. Meier and B. P. Zakharchenya.
[12] P. Li and H. Dery, Phys. Rev. Lett. **105**, 037204 (2010).
[13] J. R. Chelikowsky and M. L. Cohen, Phys. Rev. B **10**, 5095 (1974).
[14] J. R. Chelikowsky and M. L. Cohen, Phys. Rev. B **14**, 556 (1976).
[15] W. Weber, Phys. Rev. B **15**, 4789 (1977).
[16] P. Y. Yu and M. Cardona, *Fundamentals of Semiconductors: Physics and Materials Properties* (Springer Berlin Heidelberg, New York, 2005).
[17] *Numerical Data and Functional Relationships in Science and Technology*, Vol. 22, Pt. a of *Landolt-Börnstein, New Series, Group III*, edited by O. Madelung, M. Schultz, and H. Weiss (Springer-Verlag, Berlin, 1982).
[18] F. Nastos, J. Rioux, M. Strimas-Mackey, B. S. Mendoza, and J. E. Sipe, Phys. Rev. B **76**, 205113 (2007).

[19] G. Lampel, Proc. 9th Int. Conf. Phys. Semicond. **2**, 1139 (1968).
[20] A. S. Verhulst, Ph.D. thesis, Stanford University, 2004.
[21] There is a disagreement for the selection rules in silicon direct gap transition at Γ point between Lampel's original work [19] and the results of Nastos *et. al.*[18]. Our rechecked results support the latter.